

Direct transfer of light's orbital angular momentum onto non-resonantly excited polariton superfluid

Byoung Yong Oh^{1†}, Min-Sik Kwon^{1,2†}, Su-Hyun Gong^{1,2}, Je-Hyung Kim^{1,2}, Hang Kyu Kang³, Sooseok Kang³, Jin Dong Song³, Hyoungsoon Choi^{1*}, and Yong-Hoon Cho^{1,2*}

¹ Department of Physics, Korea Advanced Institute of Science and Technology (KAIST), Daejeon, Republic of Korea

² KI for the NanoCentury, Korea Advanced Institute of Science and Technology (KAIST), Daejeon, Republic of Korea

³ Center for Opto-Electronic Convergence Systems, Korea Institute of Science and Technology (KIST), Seoul, Republic of Korea

† : These authors contributed equally to this work.

*: These authors are corresponding author who contributed equally.

e-mail : h.choi@kaist.ac.kr; yhc@kaist.ac.kr

Recently, exciton-polaritons were found to condense into a coherent ground state much like a Bose-Einstein condensate and superfluid. They have become a good testbed for generating and manipulating quantum vortices in a dissipative-driven superfluid by the optical control of light-matter coupling inside a semiconductor microcavity. Here, we generate exciton-polariton condensate with non-resonant Laguerre Gaussian (LG) optical beam and verify the direct transfer of light's orbital angular momentum to exciton-polariton quantum fluid. Quantized vortices are found in spite of large energy relaxation involved in non-resonant pumping. We identified phase singularity, density

distribution and energy eigenstates for the vortex states. Our observations confirm that non-resonant optical LG beam can be used to manipulate chirality, topological charge and stability of non-equilibrium quantum fluid. It suggests that quantum information can be transferred between photon and exciton-polariton relatively easily, and they can be expanded to form the controllable network of multiple topological charges even in the presence of solid state spectral randomness.

I. INTRODUCTION

A quantum vortex, initially discovered in superconductors [1-3], superfluid helium [4-6] and cold atoms [7,8] is a topological defect resulting from a phase matching condition of rotational superflow. Due to the topological stability, it has potential applications in data storage and transfer [9-11]. Fundamentally, a quantum vortex is a signature of phase coherence in a superconductor or a superfluid carrying either a quantized magnetic flux or a quantized angular momentum, respectively. Studying the quantized vortex in exciton-polaritons has a distinct advantage over other superfluid and superconductor systems, in the sense that the system includes a photonic component which can be easily visualized [12-16]. A microcavity exciton-polariton has a finite lifetime and decays by leaking photons out of the cavity [17,18]. The leaking photon carries the momentum, energy and phase information of the polaritons. By studying the dynamics of the decaying photons, one can directly study the dynamics of the polaritons and vortices within. Their real-time evolution, including the vortex formation process in the polariton fluid, can be studied [13,19-21]. The leaky nature of photons makes the system an inherently non-equilibrium one adding another layer of intricacy in studying quantum fluids.

In its simplest form, all that is required to create quantum vortices is to rotate a superfluid above a critical velocity [6]. In a microcavity with semiconducting quantum wells (QWs), however, this process is complicated by the fact that an exciton-polariton is a system with a quasiparticle composed of an electron, a hole, and a photon [22,23]. There is more than one way to create exciton-polaritons, and it turns out that these different methods play an important role in vortex generation [24-27]. To create an exciton-polariton, one can either excite a polariton directly with a resonant photon or excite a high energy electron-hole plasma with a non-resonant photon and rely on the relaxation process to form polaritons. In resonant pumping, it has been reported that a photon's quantum state, such as energy, momentum, angular momentum, and phase, are transferred into polaritons. In such a case, it is not difficult to imagine creating a quantum vortex of orbital angular momentum (OAM) with winding number $m = \pm 1$ by transferring an OAM with $m = \pm 1$ of a photon, and that has been experimentally realized [19,28].

With non-resonant pumping the direct transfer of a photonic quantum state into a polariton condensate is considered to be non-trivial. The initially injected hot carriers create an exciton reservoir during relaxation which helps efficient cooling of polaritons into the condensation state by polariton-polariton scattering. The scatterings, however, are also susceptible to decoherence of the quantum information originally implanted in the electron-hole plasma. Instead, creating various patterns of geometrical flow is found to be effective in generating vortices. Due to the finite lifetime of polaritons, a steady state with a diffusive flow of polariton condensate can be engineered. Their unique nature allows the vortex to be generated by creating various flow patterns that are only possible in a pump-dissipation system [22-27,29] on top of more conventional schemes based on rotation [19] or turbulent flow around defects [20].

However, in this study, we show that converting OAM of a non-resonant photon into a vortex of an exciton-polariton condensate is not only possible but surprisingly robust. It is a striking result from the viewpoint of the polariton relaxation dynamics discussed earlier. Moreover, our result has more analogy to driving phase transition from a rotating normal fluid into a vortex carrying superfluid as in helium or cold atom than previous methods of generating vortices [20,25,29]. Consequently, it is considerably more advantageous in terms of controlling the number of vortices and their chirality. With a sufficiently large OAM of light, Abrikosov vortex lattice with net circulation should be possible.

Manipulating the vortex state with OAM of light is immensely simpler than finding particular geometric flow patterns to generate vortices. Furthermore, the real advantage lies in one to one correspondence between the OAM of light and topological charge of the vortex, which provides a channel for quantum information transfer between photons and polaritons. Also considering the inherent spectral randomness in semiconductor exciton-polariton systems, not having to rely on resonance alleviates a major challenge in forming a network of multiple polariton systems. Our observation sheds new light on both the vortex formation and the relaxation in semiconductor microcavity and paves the way to developing the exciton-polariton system as a platform for quantum information.

II. CREATION OF VORTEX FROM NON-RESONANTLY PUMPED ORBITAL ANGULAR MOMENTUM

Our sample consisted of GaAs QWs and distributed Bragg reflectors (DBR) structure forming a microcavity. In experiment setup, a Ti:Sapphire pulse laser with an energy of 1.73 eV (716 nm), which corresponds to the first and the largest dip outside the DBR stopband in

reflectivity curve, was our primary choice to shine onto our sample in a cryostat at 6 K (Fig. 1a). Strong light-matter coupling in the microcavity resulted in a polariton eigenstate. The energy-momentum dispersion relation of this emergent eigenstate is described in Fig. 1e. As we increased the power of the incident beam above the condensate threshold, we observed the polariton condensation at the ground state (1.59 eV) of the lower polariton branch. To make a vortex state, we used a Laguerre-Gaussian (LG) optical pump as a stirrer to induce circulation (Fig. 1d). A phase mask was used to convert the Gaussian mode beam of a pulsed laser into an LG beam with $m = \pm 1$ and ± 2 (OAM) (Fig. 1a). Spatial intensity distribution and interference were measured in the Michelson interferometer integrated with a Fourier optics imaging setup [30].

Fig. 1b shows the spatial intensity distribution (Fig. 1b left) and interference (Fig. 1b right) of the laser pump beam at 3 mW (2 times the threshold power) reflected from the sample. Its spot size is about 30 μm . The spatial interference of the polaritons indicates the creation of long-range coherence and quantized vortices in Fig. 1c,d. Interference images were measured by Michelson interferometer to check the spatial correlation of coherent regions. Magnified images in Fig. 1c,d were extracted by Fourier filtering in a computer program for clarity of interference pattern.

In Fig. 1c, d, the images show the Michelson interference of the emission of polaritons below (Fig. 1c) and above (Fig. 1d) the threshold power pumped by the LG beam ($m = +1$). The interference pattern indicates the presence of spatial phase coherence in the polariton state. Above the threshold power, two noticeable effects occurred. One, the spatial correlation region with coherence expanded in the area from about 200 μm^2 (Fig. 1c) to 700 μm^2 (Fig. 1d), which shows long-range coherence as a result of the polariton condensate. Two, there is a 2π phase winding marked by a fork shape dislocation in the interference pattern, which is direct evidence

of the formation of the quantum vortex.

In the low density regime (below threshold), a small region of the interference pattern with no anomaly (Fig. 1c) exhibited short range correlation, stemming from the correlation length of the thermal de Broglie wavelength of the polaritons. In the higher density regime, the thermal de Broglie wavelength of the polaritons becomes comparable to their average separation. After cooling through spontaneous and stimulated polariton-polariton scattering, a polariton condensate and superfluidity with long-range interference is formed. The polariton condensate can build a quantized circulation. It then shows a single quantum vortex with a 2π phase winding when excited by a photon with OAM of $m = + 1$ in the Fig. 1d. A fork-shaped dislocation appears clearly in the interference pattern [19,31,32]. Because of the retro-reflector in the Michelson interferometer, an artifact, the fork on the right side among the fork dislocation pair is created as shown in the magnified image in Fig. 1d. Above the condensation threshold, ground and excited states of the condensate with a single vortex were measured as shown in Fig. 1f.

Additional experiments were carried out to confirm that the quantized vortices are a result of the orbital angular momentum transfer of a non-resonant excitation.

III. CHIRALITY DEPENDENCE

The simplest test to see if the angular momentum of the light is transferred to the quantum vortex is to compare the phase winding direction of the vortex to that of the incident beam. The Michelson interferometer setup was not straightforward, because the interference image always contained two fork images in opposite directions, one from the vortex and another from the retro-reflection of that same vortex. Even when we flipped the OAM of the incident laser, the

resulting image would again contain vortices with $+2\pi$ and -2π phase winding.

To confirm whether the phase winding direction of the emission from the polariton was identical to that of the incident laser, a modified Mach-Zehnder (MZ) interferometry was constructed (for details, see Ref [33]). In this set up, a vortex was contained only in one arm of the interferometer, and the direction of the phase winding could be identified. Fig. 2 shows interference patterns both from the laser and emission, and we found that their phase winding directions are identical to each other. In other words, when the laser with an OAM $m = +1$ is injected, a fork-shaped interference pattern is seen from the reflection. The interference pattern of the emission beam also shows a fork-shape indicating that the quantized vortex also carries an angular momentum of $m = +1$. When the incident beam's angular momentum was flipped to $m = -1$, the emission from the polariton condensate also flipped its angular momentum suggesting that the vortex was a result of the incident beam's angular momentum.

IV. INCIDENT ORBITAL ANGULAR MOMENTUM DEPENDENCE

To further rule out the possibility of other causes for the vortex formation, we repeated the measurement with different angular momentum values at the same pump power ($1.6 P_{th}$). To get a ring-shaped beam of $m = 0$, we inserted a circular block in the image plane of the laser. The beam block was designed such that the inner diameters of the circular beam were similar to the size to our LG beam.

When an $m = 0$ circular beam was injected, no dislocation in interference pattern was observed. Previous studies have reported that a diffusive geometric flow from a blueshifted potential landscape or defects in the sample can result in vortices [12,25]. Diffusive flow pattern can be obtained from the spatial phase distribution (Fig. 3c). Phase gradient in the radial

direction is clearly present as a result of a difference in polariton density along the radius, which creates a diffusive flow. Since the incident beam was ring shaped, the polariton density was the highest around the ring-shaped pumped region, and phase gradient was present both inside and outside the ring as expected. The absence of a vortex for $m = 0$ indicates that transfer of phase winding for $m \neq 0$ was responsible for the vortex formation and not the diffusive flow or defects.

With an OAM of $m = +1$ incident beam, the spatial intensity of the emission was largely unaffected. However, fork in the interference pattern appeared around the dark region in the center of the ring (Fig. 3e). Again, two forks in the opposite direction appeared as a result of interference with a retro-reflected beam in the Michelson interferometer. In addition to the radial phase gradient, a 2π azimuthal phase winding is present around the fork (Fig. 3f). When the OAM of the incident laser was increased to $m = +2$, a total of four forks, two in each direction, were seen in the emission (Fig. 3h). Two single quantized vortices were generated, consistent with what was expected for a superfluid. The total angular momentum of the injected beam was preserved in this test.

V. STABILITY OF VORTICES WITH INCREASING EXCITATION POWER OF ORBITAL ANGULAR MOMENTUM

In order to detect the stability of the polariton vortex, we increased the polariton-polariton interaction by raising the incident pumping power in the polariton condensate. As stated earlier, a higher laser intensity led to an increase in the number of excitons and polaritons. The polariton density and optically induced effective potential change as the optical pumping power

varies. Therefore, it may affect the vortex stability.

Fig. 4 shows that the polariton vortices and condensates for each transferred angular momentum ($m = 0, 1$, and 2) are excited by varying the pumping power (for details, see Ref [33]). In Fig. 4a-d, at powers of (a) $1.4 P_{th}$, (b) $2.3 P_{th}$, (c) $11.4 P_{th}$ and (d) $31.8 P_{th}$ the spatial interference of the ring-shaped polariton condensates ($m = 0$) were measured without any clear signal of vortices (no fork dislocation in the interference image). Close to a pump power of $31.8 P_{th}$, clarity in the spatial interference was weakened due to decreased coherence, which originates with the polariton-polariton interaction at higher pump density (Fig. 4d). No spontaneously formed vortex was seen in the $m = 0$ ring-shaped beam even with high pump power (Fig. 4a-d). From these results, we can comprehend that the interplay between sample inhomogeneity and polariton flow in optically induced potential are negligible in the pumped region of the sample.

For the LG pump beam with winding number $m = 1$, shown in Fig. 4e-h, a single vortex appeared above the threshold $1.2 P_{th}$, (Fig. 4e) and was stably maintained in the center of the LG pump area up to a pump power of $\sim 10 P_{th}$ (Fig. 4f,g). Above the $10 P_{th}$ pump density, a single vortex became unstable, inducing the phase fluctuation shown in the weakened clarity of the spatial interference. When the pumping power was as high as $30 P_{th}$ no clear vortices were shown, which could be a result of the flow and interaction (turbulence) of higher density polaritons with an optically induced potential (Fig. 4h).

In Fig. 4i-l, two vortices were created by the LG pump beam with $m = 2$, and they were stable up to a pump power of $3 P_{th}$ (Fig. 4i and 4j). Above $3 P_{th}$, additional vortices appeared in the ring-shaped pumped region. When the pump power was further increased beyond $10 P_{th}$, an obscure interference pattern occurred and the vortices disappeared; its origin may be identical

to what's seen in the $m = 1$ case with $P > 10 P_{\text{th}}$ (Fig. 4k,l).

The instability in vortex formation at higher pumping density is related to the change in potential landscape, which affects the flow condition of the polaritons. It also seems that the polariton vortex generated from the transferred OAM has a stable regime (dashed box in Fig. 4), which is maintained while the non-resonant pumping density increases, before entering a higher power regime. In the reference [28], a polariton vortex was created by an optical parametric oscillator (OPO) pump and an $m = 1$ phase winding imprinting beam. A single vorticity was maintained while pump power was increased to $4.5 P_{\text{th}}$. In our experiment, the $m = 1$ vortex was stable up to a higher pump power [28].

In addition, the vortex maintained even with asymmetry in the intensity of the ring-shaped beam up to a point (for details, see Ref [33]). Vortices also remained stable with the change in pump beam radius as much as 30% (for details, see Ref [33]). All of these show the robustness of vortex formation by transferring OAM of the non-resonant pump beam.

VI. DISCUSSION

In this work, we have demonstrated that vortices in polariton condensate can be created by transferred orbital angular momentum of a non-resonant pump beam. Conservation of both chirality and total angular momentum ($m = 0, 1, \text{ and } 2$) between the incident light and the quantized vortices in polariton condensates, even in high interaction regime at pump power way above the threshold value, is shown. This is the first demonstration of the optical phase winding directly transferred onto polariton condensate formed from electron-hole plasma with high energies going through scatterings among electrons, holes, excitons and polaritons.

We considered two different mechanisms, parametric scattering or pumping memory effect, as viable explanations for what we observed. First, we noticed that the primary absorption dip in our DBR stopband (1.73 eV) is 144 meV above the condensed ground state energy of 1.59 eV. This happens to be almost exactly four times the longitudinal optical (LO) phonon energy of 36 meV in GaAs. If some unknown parametric scattering channel is available involving four LO phonons either sequentially or simultaneously, polaritons may reach its ground state conserving the initial angular momentum imposed onto the system. To test this scenario, we tuned our incident laser from 1.70 eV to 1.77 eV. Quantized vortices are found when the energy of the pump beam is not an exact multiple of the LO phonon energy, suggesting that parametric scattering by LO phonons is unlikely to be the dominant process.

This leaves us with pumping memory effect. In the past, spin angular momentum, i.e. circular polarization of a non-resonant pump beam is found to be preserved through the competition between transferred optical spin and relaxation process, which is known as the optical spin memory effect [34,35]. What we are seeing could be interpreted as a similar effect where the orbital angular momentum transferred incidentally from pump beam is conserved down to the polariton ground state through stimulated scattering [36-38]. Keeling *et al.*[22] proposed that when the pumping spot is larger than the Thomas-Fermi cloud, the circular symmetry of polaritons flowing towards the center of a harmonic trap becomes unstable and non-zero net circulation and vortex array can be generated. In such a scenario, circular symmetry is spontaneously broken. Injection of angular momentum with an LG beam could nudge the polariton fluid to follow the chirality and angular momentum of the incident beam, resulting in the pumping memory effect. However, microscopic details are lacking and this warrants additional investigations of this subject. Especially, an advanced theoretical model describing relaxation of carriers, excitons, and polaritons could guide future experimental

efforts.

In conclusion, we transferred optical phase winding onto polaritons by using only phase masks (vortex lens) without additional probe (trigger) beam nor angle-dependent optical pumping for direct injection of polaritons (resonant pumping, for details, see Ref [33]). Excellent controllability of polariton OAM through a simple manipulation of incident light's OAM provides a new and powerful method for studying all optical memory devices [39,40], such as vortex memory [41], and simple quantum simulators [42-44].

ACKNOWLEDGEMENT

The authors wish to thank L.S. Dang, M. Richard (CNRS, Grenoble, France), I. Savenko (IBS, Daejeon, Republic of Korea), C. Park and M. Kim (KAIST, Daejeon, Republic of Korea) for helpful discussions. This research was supported by National Research Foundation (NRF) of Korea through projects NRF-2016R1A2A1A05005320, 2015R1C1A1A01055813 and 2016R1A5A1008184, and the Climate Change Research Hub of KAIST (Grant No.N11160013). The authors in KIST acknowledge the support from KIST institutional program of flagship.

APPENDICES

APPENDIX A: SAMPLE

A semiconductor sample consisting of QWs, a microcavity, and DBR was made by molecular beam epitaxy (MBE) growth. A $\lambda/2$ AlAs cavity was sandwiched between two AlAs/AlGaAs distributed Bragg reflectors, with 16 and 20 pairs for the top and bottom components, respectively. The GaAs multiple-QWs were located at the three antinodes of the electric field

of a cavity to increase spatial overlap between the exciton and the electric fields. The strong coupling regime was confirmed by both reflectivity and E-k dispersion curve measurement. The measurements showed a Rabi splitting of $2\hbar\Omega_R = 17.8$ meV. They indicated photon-exciton detuning $\delta = 0.5$ meV, which are estimated by fitting the energy momentum dispersion curve.

APPENDIX B: EXPERIMENT SETUP

We performed the experiment with a non-resonant pump scheme, using a mode-locked Ti:Sapphire pulse laser with an energy of 1.73 eV (716 nm) with a 150 fs pulse width and 80 MHz repetition rate. The incident direction of the pump was normal to the sample surface ($k_{\parallel} = 0$).

For the stable exciton-photon strong coupling regime, it was necessary to decrease the temperature to 6 K using a cryostat. The cryostat had a closed cycle of helium flow and vibration free system. The sample was mounted on a copper sample holder by using silver paste. A piezo stage in the cryostat was used to provide accurate control of position for the sample.

In optical setup, a high numerical aperture (0.55) objective lens was used to make excitation pumping spot on the sample, and collect the emission from exciton-polariton condensate. We obtained the momentum, energy and real space information of polaritons simultaneously using a Fourier microscope combined with a monochromator and charge-coupled device (CCD) camera [45]. To form the OAM of the pump beam, we used a phase mask, whose structure is made of helical phase steps. The phasemask transferred the Gaussian pump beam profile to the LG beam with OAM. For comparing the presence with

the absence of transferred OAM in polariton condensates (Fig. 3), we made a ring shaped beam without angular momentum ($m = 0$) by using a $10 \mu\text{m}$ chromium mask on a glass plate. To clearly observe the location and distribution of vortices, a Michelson interferometer was installed in the detection part. One arm of the interferometer had a retroreflector for direct measurement of the spatial correlation distribution ($g^{(1)}$ distribution).

REFERENCES

- [1] A. A. Abrikosov, *Magnetic properties of superconductors of the second group*. Soviet Phys. JETP **5**, 1174 (1957).
- [2] M. Tinkham, *Introduction to Superconductivity*. (McGraw-hill Book Co., New York, 1996).
- [3] U. Essmann and H. Träuble, *The direct observation of individual flux lines in type II superconductors*. Physics Letters A **24**, 526 (1967).
- [4] W. F. Vinen, *Detection of single quanta of circulation in rotating helium II*. Nature **181**, 1524 (1958).
- [5] G. A. Williams and R. E. Packard, *Photographs of Quantized Vortex Lines in Rotating He II*. Phys. Rev. Lett. **33**, 280 (1974).
- [6] E. J. Yarmchuk, M. J. V. Gordon and R. E. Packard, *Observation of Stationary Vortex Arrays in Rotating Superfluid Helium*. Phys. Rev. Lett. **43**, 214 (1979).
- [7] K. W. Madison, F. Chevy, W. Wohlleben and J. Dalibard, *Vortex Formation in a Stirred Bose-Einstein condensate* Phys. Rev. Lett. **84**, 806 (2000).
- [8] J. R. Abo-Shaer, C. Raman, J. M. Vogels and W. Ketterle, *Observation of Vortex Lattices in Bose-Einstein Condensates*. Science **292**, 476 (2001).
- [9] N. Y. Yao, C. R. Laumann, A. V. Gorshkov, H. Weimer, L. Jiang, J. I. Cirac, P. Zoller and M. D. Lukin, *Topologically protected quantum state transfer in a chiral spin liquid*. Nat. Commun. **4**, 1585 (2013).
- [10] X. Ma and S. Schumacher, *Vortex-vortex control in exciton-polariton condensates*. Phys. Rev. B **95**, 235301 (2017).
- [11] Y. Paltiel, E. Xeldov, Y. N. Myasoedov, H. Shtrikman, S. Bhattacharya, M. J. Higgins, Z. L. Xiao, E. Y. Andrei, P. L. Gammel and D. J. Bishop, *Dynamic instabilities and memory effects in vortex matter*. Nature **403**, 398 (2000).
- [12] K. G. Lagoudakis, M. Wouters, M. Richard, A. Baas, I. Carusotto, R. André, Le Si Dang and B. Deveaud-Plédran, *Quantized vortices in an exciton-polariton condensate*. Nat. Phys. **4**, 706 (2008).
- [13] F. Manni, K. G. Lagoudakis, T. C. H. Liew, R. André, V. Savona and B. Deveaud, *Dissociation dynamics of singly charged vortices into half-quantum vortex pairs*. Nat. Commun. **3**, 2310 (2012).
- [14] G. Tosi, F. M. Marchetti, D. Sanvitto, C. Antón, M. H. Szymańska, A. Berceanu, C. Tejedor, L. Marrucci, A. Lemaître, J. Bloch and L. Viña, *Onset and Dynamics of Vortex-Antivortex Pairs in Polariton Optical Parametric Oscillator Superfluids*. Phys. Rev. Lett. **107**, 036401 (2011).
- [15] G. Roumpos, M. D. Fraser, A. Löffler, S. Höfling, A. Forchel and Y. Yamamoto, *Single vortex-antivortex pair in an exciton-polariton condensate*. Nat. Phys. **7**, 129 (2011).
- [16] F. Manni, T. C. H. Liew, K. G. Lagoudakis, C. Ouellet-Plamondon, R. André, V. Savona and B. Deveaud, *Spontaneous self-ordered states of vortex-antivortex pairs in a polariton condensate*. Phys. Rev. B **88**, 201303 (2013).
- [17] H. Deng, H. Haug and Y. Yamamoto, *Exciton-polariton Bose-Einstein condensation*. Rev. Mod. Phys. **82**, 1489 (2010).
- [18] I. Carusotto and C. Ciuti, *Quantum fluids of light*. Rev. Mod. Phys. **85**, 299 (2013).
- [19] D. Sanvitto, F. M. Marchetti, M. H. Szymańska, G. Tosi, M. Baudisch, F.P. Laussy, D. N. Krizhanovskii, M. S. Skolnick, L. Marrucci, A. Lemaître, J. Bloch, C. Tejedor and L. Viña, *Persistent currents and quantized vortices in a polariton superfluid*. Nat. Phys.

- 6, 527 (2010).
- [20] G. Nardin, G. Grosso, Y. Léger, B. Piętko, F. Morier-Genoud and B. Deveaud-Plédran, *Hydrodynamic nucleation of quantized vortex pairs in a polariton quantum fluid*. Nat. Phys. **7**, 635 (2011).
 - [21] K. G. Lagoudakis, F. Manni, B. Pietka, M. Wouters, T. C. H. Liew, V. Savona, A. V. Kavokin, R. André and B. Deveaud-Plédran, *Probing the Dynamics of Spontaneous Quantum Vortices in Polariton Superfluids*, Phys. Rev. Lett. **106**, 115301 (2011).
 - [22] J. Keeling and N. G. Berloff, *Spontaneous rotating vortex lattices in a pumped decaying condensate*. Phys. Rev. Lett. **100**, 250401 (2008).
 - [23] M. O. Borgh, G. Franchetti, J. Keeling and N. G. Berloff, *Robustness and observability of rotating vortex lattices in an exciton-polariton condensate*. Phys. Rev. B **86**, 035307 (2012).
 - [24] D. Sanvitto, S. Pigeon, A. Amo, D. Ballarini, M. D. Giorgi, I. Carusotto, R. Hivet, F. Pisanello, V. G. Sala, P. S. S. Guimaraes, R. Houdré, E. Giacobino, C. Ciuti, A. Bramati and G. Gigli, *All-optical control of the quantum flow of a polariton condensate*. Nat. Photon. **5**, 610 (2011).
 - [25] R. Dall, M. D. Fraser, A. S. Desyatnikov, G. Li, S. Brodbeck, M. Kamp, C. Schneider, S. Höfling and E. A. Ostrovskaya, *Creation of Orbital Angular Momentum States with Chiral Polaritonic Lenses*. Phys. Rev. Lett. **113**, 200404 (2014).
 - [26] T. Boulier, H. Terças, D. D. Solnyshkov, Q. Glorieux, E. Giacobino, G. Malpuech and A. Bramati, *Vortex chain in a resonantly pumped polariton superfluid*. Sci. Rep. **5**, 9230 (2015).
 - [27] T. Boulier, E. Cancellieri, N. D. Sangouard, Q. Glorieux, A. V. Kavokin, D. M. Whittaker, E. Giacobino and A. Bramati, *Injection of Orbital Angular Momentum and Storage of Quantized Vortices in Polariton Superfluids*. Phys. Rev. Lett. **116**, 116402 (2016).
 - [28] D. N. Krizhanovskii, D. M. Whittaker, R. A. Bradley, K. Guda, D. Sarkar, D. Sanvitto, L. Vina, E. Cerda, P. Santos, K. Biermann, R. Hey and M. S. Skolnick, *Effect of interactions on vortices in a nonequilibrium polariton condensate*. Phys. Rev. Lett. **104**, 126402, (2010).
 - [29] G. Tosi, G. Christmann, N. G. Berloff, P. Tsotsis, T. Gao, Z. Hatzopoulos, P. G. Savvidis and J. J. Baumberg, *Geometrically locked vortex lattices in semiconductor quantum fluids*. Nat. Commun. **3**, 2255 (2012).
 - [30] J. Kasprzak, M. Richard, S. Kundermann, A. Baas, P. Jeambrun, J. M. J. Keeling, F. M. Marchetti, M. H. Szymańska, R. André, J. L. Staehli, V. Savona, P. B. Littlewood, B. Deveaud and L. S. Dang, *Bose-Einstein condensation of exciton polaritons*. Nature **443**, 409-414 (2006).
 - [31] M. R. Matthews, B. P. Anderson, P. C. Haljan, D. S. Hall, C. E. Wieman and E. A. Cornell, *Vortices in a Bose-Einstein Condensate*. Phys. Rev. Lett. **83**, 2498 (1999).
 - [32] L. P. Pitaevskii and S. Stringari, *Bose-Einstein Condensation*. (Clarendon Press, 2003).
 - [33] Supplementary materials.
 - [34] R. I. Dzhioev, V. L. Korenev, I. A. Merkulov and B. P. Zakharchenya, *Manipulation of the Spin Memory of Electrons in n-GaAs*. Phys. Rev. Lett. **88**, 256801 (2002).
 - [35] M. J. Snelling, A. S. Plaut, G. P. Flinn, A. D. Tropper and R. T. Harley, *Spin relaxation in optically excited quantum wells*. Journal of Luminescence **45** 208 (1990).
 - [36] M. D. Martin, G. Aichmayr, L. Vina and R. Andre, *Polarization control of the nonlinear emission of semiconductor microcavities*. Phys. Rev. Lett. **89**, 077402 (2002)

- [37] F. J. Rodríguez, L. Quiroga, C. Tejedor, M. D. Martín and L. Viña, *Polariton relaxation dynamics in semiconductor microcavities: Non-Markovian effects*. AIP Conf. Proc. **893**, 1151 (2007)
- [38] M. D. Martin, G. Aichmayr, A. Amo, D. Ballarini, Ł Kłopotowski and L. Viña, *Polariton and spin dynamics in semiconductor microcavities under non-resonant excitation*. J. Phys.: Condens. Matter **19**, 295204 (2007)
- [39] T. Byrnes, N. Y. Kim and Y. Yamamoto, *Exciton polariton condensates*, Nat. phys. **10**, 803 (2014).
- [40] C. Schneider, K. Winkler, M. D. Fraser, M. Kamp, Y. Yamamoto, E. A. Ostrovskaya and S. Höfling, *Exciton-polariton trapping and potential landscape engineering*. Rep. Prog. Phys. **80**, 016503 (2014).
- [41] H. Sigurdsson, O. A. Egorov, X. Ma, I. A. Shelykh and T. C. H. Liew, *Information processing with topologically protected vortex memories in exciton-polariton condensates*. Phys. Rev. B **90**, 014504 (2014).
- [42] G. Tosi, G. Christmann, N. G. Berloff, P. Tsotsis, T. Gao, Z. Hatzopoulos, P. G. Savvidis and J. J. Baumberg, *Sculpting oscillators with light within a nonlinear quantum fluid*. Nat. Phys. **8**, 190 (2012).
- [43] H. Ohadi, R. L. Gregory, T. Freearge, Y. G. Rubo, A. V. Kavokin, N. G. Berloff and P. G. Lagoudakis, *Nontrivial Phase Coupling in Polariton Multiplets*. Phys. Rev. X **6**, 031032 (2016).
- [44] I. Buluta and F. Nori, *Quantum simulators*. Science **326**, 108 (2009).
- [45] M. Richard, J. Kasprzak, R. André, R. Romestain and L. S. Dang, *Experimental evidence for nonequilibrium Bose condensation of exciton polaritons*. Phys. Rev. B **72**, 201301 (2005).

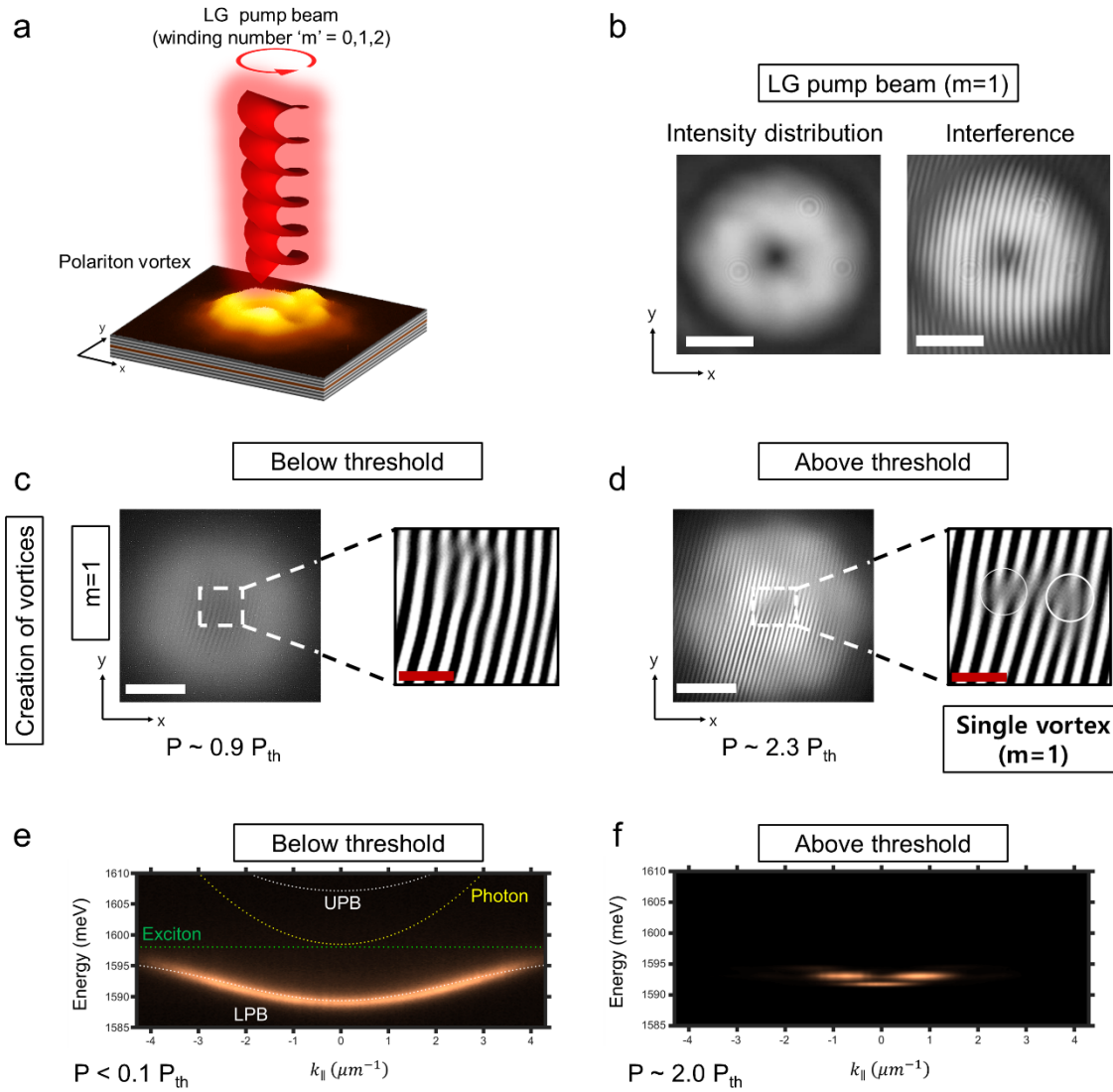


FIG. 1. Creation of a vortex using non-resonant pumping by transfer of OAM (phase winding). (a) Schematic configuration of vortex optically pumped with OAM (phase winding) in real space. (b) Spatial distribution of the intensity (left) and spatial interference (right) of the LG laser beam with 2π phase winding ($m = +1$). The interference image was measured by MZ interferometer for identification of a vortex. (c,d) Creation of a single quantized vortex in non-resonant LG beam pumping with $m = +1$ winding number. Spatial interference of polaritons below the threshold in c and a single polariton vortex (topological charge $m = +1$) above the threshold pump power of a polariton condensate in d. Above the threshold, fork dislocations

were clearly shown (white circles) in the magnified figure in d, but before the threshold, there was no fork dislocation in the magnified figure in c. (e) Energy-momentum dispersion of lower polariton branch (LPB) measured by angle-resolved photoluminescence setup below the condensation threshold. UPB: Upper polariton branch (fitted curve, white, dotted). Parabolic (yellow, dotted) and flat dispersion (green, dotted) indicate cavity photon and exciton dispersion fitting, respectively. (f) The ground and first excited states above the condensation threshold. Scale bars, $10\ \mu\text{m}$ (white), $2.5\ \mu\text{m}$ (red).

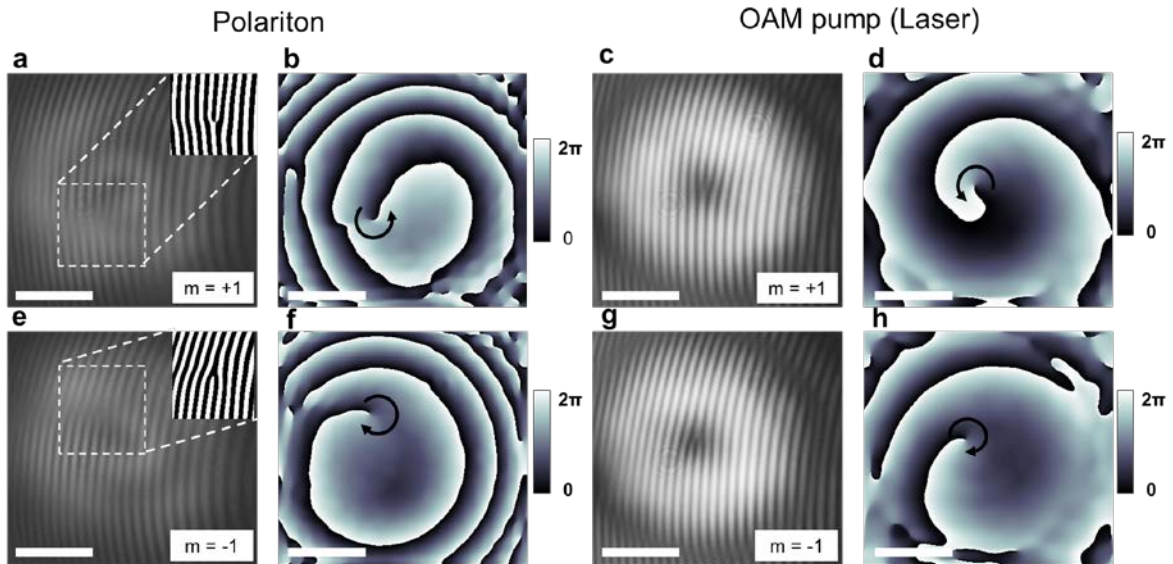


FIG. 2. Chirality dependence of polariton vortex and incident laser beam. (a-d) The incident pump beam has the OAM, $m = +1$. (a) Interference image and (b) phase image of the polariton vortex extracted from a, showing a phase winding pattern in the counter clockwise direction ($m = +1$). (c) Interference image and (d) phase image of the pumped beam with the counter clockwise phase winding. (e-h) The incident pump beam has the OAM, $m = -1$. Directions of the phase winding for both the polariton vortex and laser beam are clockwise ($m = -1$). The clearly striped patterns on the upright of (a) and (e) were extracted from the dotted box regions in (a) and (e), respectively. A modified MZ interferometer was used. Scale bars are $10\ \mu\text{m}$.

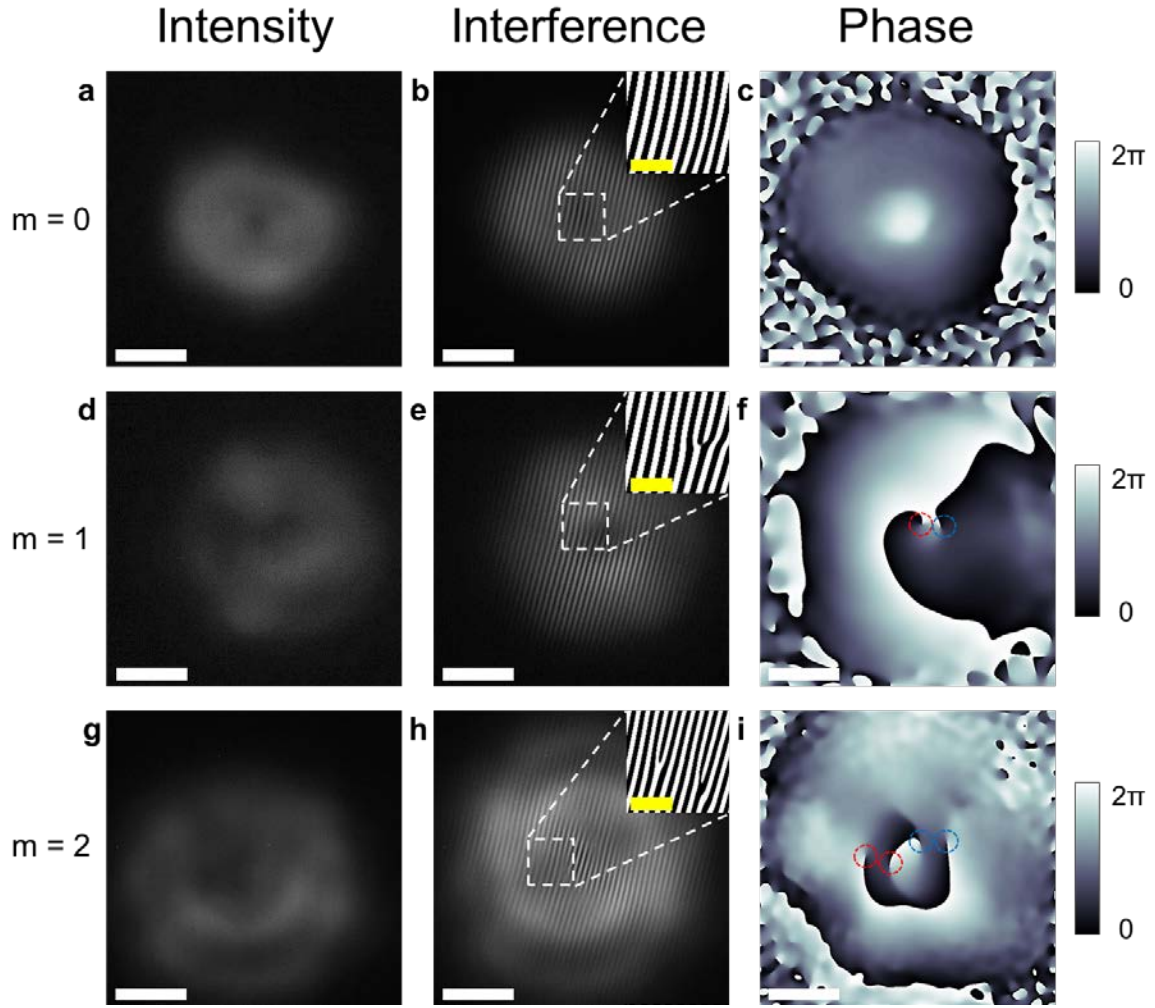


FIG. 3. Dependence of winding number on incident orbital angular momentum. The OAM of vortices induced by the OAM of a pump laser from $m = 0$ to $m = +2$. Polariton image and Michelson interference image using both a mirror and retroreflector. (a-c) (first row) A ring-shaped beam without OAM ($m = 0$) was used as the pump beam. (a) Image of a polariton for $m = 0$. In (b), the interference image only has a striped pattern in the polariton region, and no vortex is observed. (c) Phase winding did not exist in the density distribution of polariton. (d-f) (second row) The incident ring beam has the OAM ($m = +1$). (d) Image of a polariton at $m = +1$. (e) A pair of fork patterns is clearly seen in the interference image. (f) A pair of the phase windings from 0 to 2π in the extracted phase map. The red circle is a real vortex, and the blue circle was induced by the reflected image of the retroreflector. (g-i)

(third row) The OAM of the pump laser beam is $m = +2$. (g) Image of a polariton at $m = +2$. (h) Two pairs of vortices are observed in the interference image. (i) The extracted phase image shows two pairs of phase winding patterns in the center of the coherent region. The stripe patterns on the upright of (b), (e) and (h) were extracted from the dotted box regions in (b), (e) and (h), respectively. All of these experiments in Fig.3 were carried out at $1.6 P_{th}$. The white and yellow scale bars are $10 \mu\text{m}$ and $2.5 \mu\text{m}$.

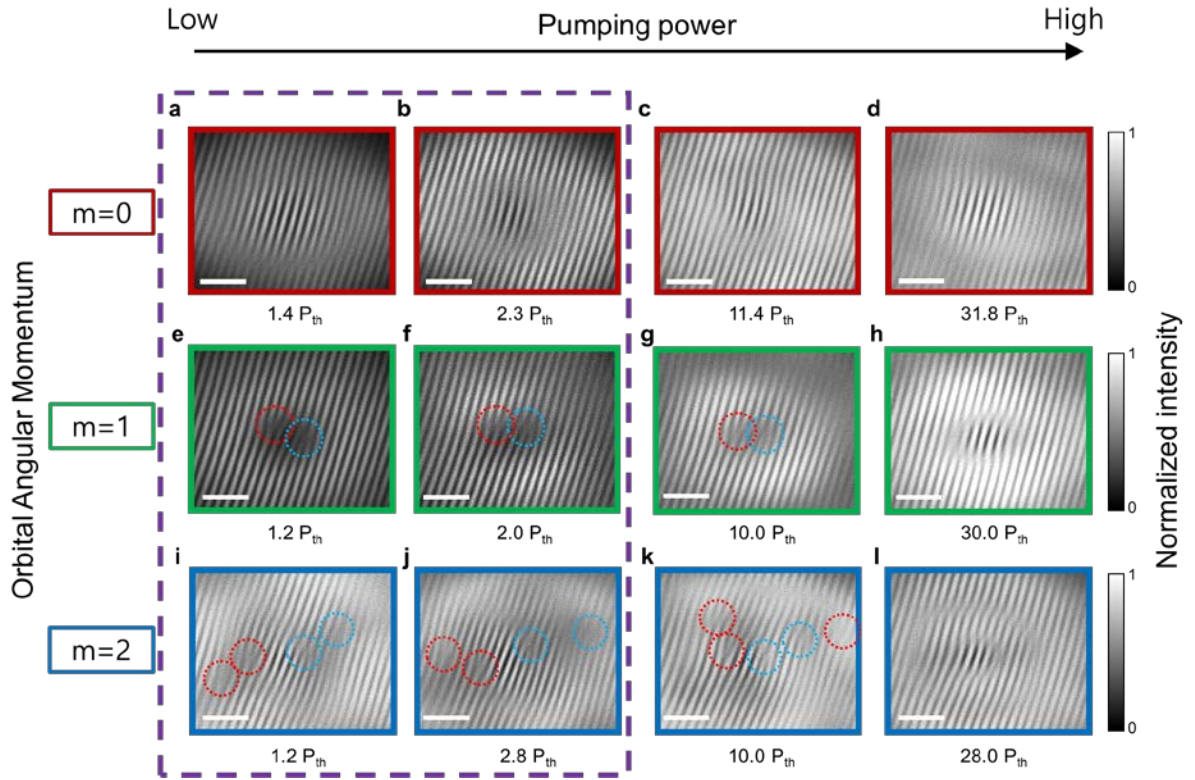


FIG. 4. Stability of the polariton vortices with topological charge $m = +1$ and $+2$ while varying pumping power. Spatial interference images of the polariton condensates generated by non-resonant pumping with (a-d) $m = 0$, (e-h) $m = +1$ and (i-l) $m = +2$ with increasing threshold pumping powers. (a-d) Polariton condensate ($m = 0$) with increasing pump power up to $31.8 P_{th}$. (e-h) A single vortex ($m = +1$) after increasing pump power up to $10.0 P_{th}$. Spatial interference images of the polariton vortex generated by non-resonant pumping with the $m = +1$ phase winding with threshold pump powers of $1.2 P_{th}$, $2.0 P_{th}$, $10.0 P_{th}$, and $30.0 P_{th}$. (i-l) Maintenance of two $m = 1$ vortices while increasing pump power up to $2.8 P_{th}$. Spatial interference images of polariton vortices generated by non-resonant pumping with $m = 2$ phase winding at threshold pump powers of $1.2 P_{th}$, $2.8 P_{th}$, $10.0 P_{th}$, and $28.0 P_{th}$. The dashed box indicates the stable regime of the vortices for the pumping power. Scale bars, $5 \mu\text{m}$.

**Direct transfer of light's orbital angular momentum onto non-resonantly excited
polariton superfluid**

Supplemental material

Byoung Yong Oh^{1†}, Min-Sik Kwon^{1,2†}, Su-Hyun Gong^{1,2}, Je-Hyung Kim^{1,2}, Hang Kyu Kang³, Sooseok Kang³, Jin Dong Song³, Hyoungsoon Choi^{1*}, and Yong-Hoon Cho^{1,2*}

¹ Department of Physics, Korea Advanced Institute of Science and Technology (KAIST), Daejeon, Republic of Korea

² KI for the NanoCentury, Korea Advanced Institute of Science and Technology (KAIST), Daejeon, Republic of Korea

³ Center for Opto-Electronic Convergence Systems, Korea Institute of Science and Technology (KIST), Seoul, Republic of Korea

† : These authors contributed equally to this work.

*: These authors are corresponding author who contributed equally.

e-mail : h.choi@kaist.ac.kr; yhc@kaist.ac.kr

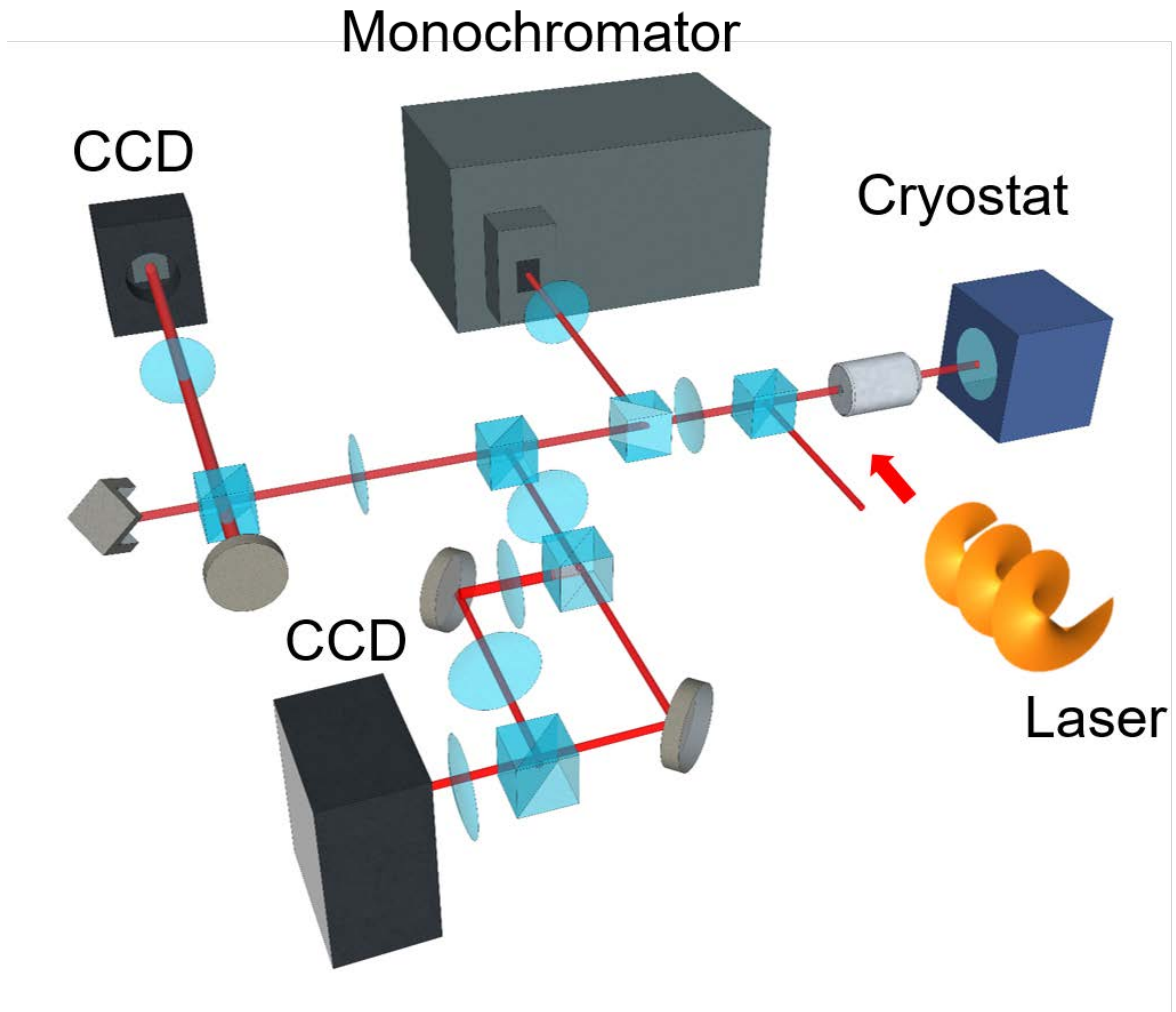


FIG. 1. Schematic of experimental setup. Angle-resolved photoluminescence (PL) with Michelson interferometer and modified Mach-Zehnder (MZ) interferometer. The incident pump beams were pulsed Ti:Sapphire laser beams. Laguerre-Gaussian (LG) beam with orbital angular momentum (OAM, winding number $m = +1$ and $+2$) and doughnut beam without OAM ($m = 0$) was used. The phase mask converts the Gaussian beam to the LG beam.

I. EXPERIMENT SETUP

To distinguish between laser and sample luminescence, we used a spectral filter and a dichroic mirror. Because of the filter setup in the measurement section, the laser and luminescence could be distinguished, so that laser intensity was cut to 0.002% of its original intensity.

To examine the extent of the spatial phase coherence of the polariton fluid, a Michelson interferometer was used. One arm of the split beam from the sample went through a retroreflector to produce a centrosymmetric inversion image of the original beam. The other arm of the split beam had a motorized stage for accurate control of the path

difference. The interference fringe in this setup represents the phase coherence between a region of the polariton fluid and its centrosymmetrically inverted region, and thus spatial correlation (i.e., $g^{(1)}$ distribution) could be directly obtained.

The Michelson interferometry had one shortcoming in identifying the chirality of the quantum vortices. Two arms of each split beam contained an image of a vortex, one upright and the other retroreflected. When these beams interfered with each other, the interference pattern always showed a vortex and an anti-vortex pair-like image for a single vortex.

To avoid this confusion, a modified Mach-Zehnder (MZ) interferometer was also set up. One arm had two convex lenses to magnify the image, and the other arm had no lens pairs. A small region of the magnified beam could be chosen such that the phase within the region was relatively uniform compared to the original phase winding beam. By interfering this uniform phase region with the original phase winding beam, one could obtain the interference pattern of a single vortex, and we were able to confirm that the phase winding direction of the polariton vortex followed that of the incident laser.

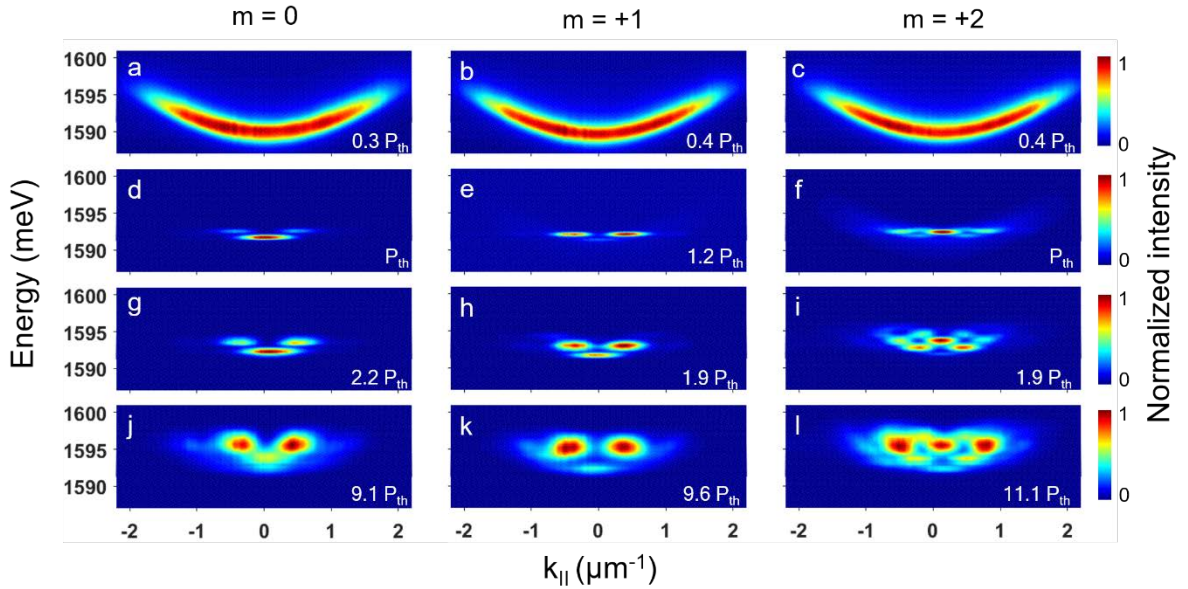


FIG. 2. Power dependence of angle-resolved photoluminescence. (a,d,g,j) Energy-momentum dispersions of the ring polariton condensate under non-resonant pumping without phase winding ($m = 0$) at varying pump powers: $0.3 P_{th}$ in a, $1.0 P_{th}$ in d, $2.2 P_{th}$ in g, $9.1 P_{th}$ in j. (b,e,h,k) Energy-momentum dispersions of $m = 1$ vortex under non-resonant pumping with phase winding ($m = 1$) at varying pump powers: $0.4 P_{th}$ in b, $1.2 P_{th}$ in e, $1.9 P_{th}$ in h, $9.6 P_{th}$ in k. (c,f,i,l) Energy-momentum dispersions of two $m = 1$ vortices under non-resonant pumping with phase winding ($m = 2$) at varying pump powers: $0.4 P_{th}$ in c, $1.0 P_{th}$ in f, $1.9 P_{th}$ in i, $11.1 P_{th}$ in l. Every image was detected at the same sample region.

Due to the numerical aperture ($NA = 0.55$) of the objective lens, the in-plane momentum range is from $-2.2 \mu\text{m}^{-1}$ to $2.2 \mu\text{m}^{-1}$.

II. DISPERSION CURVE WITH ANGULAR MOMENTUM

To check the energy of the vortex states, we measured the dispersion curve using angle-resolved photoluminescence. Below the threshold power for condensation, regardless of the phasemask presence, all dispersion curves are identically parabolic showing a free-particle-like polariton dispersion, from which the polariton effective mass was extracted and determined to be $8 \times 10^{-5} m_e$. Here m_e is the bare electron mass.

The ground state energies were also found to be identically 1590 meV. (Fig. 2a-c.) Above the threshold power, however, the presence of phasemasks dramatically alters the dispersion curve. Without the vortex formation, one would expect polaritons to condense into the zero momentum state. With vortex formation, the predominant condensed state is a finite momentum state, not the zero momentum state. This can be seen by comparing Fig. 2d-f slightly above the threshold power. In the case of $2P_{\text{th}}$, the discrete state can be seen more clearly (Fig. 2g-i). Specifically, in the case of $m = 1$ and 2 , it can be seen that a higher state is generated compared to the case of P_{th} (Fig. 2h,i). Also, this discrete state is shown to maintain well when power up to $11P_{\text{th}}$ is applied (Fig. 2j-l).

In the $m = 1$ and $m = 2$ cases, the excited state population was larger than the ground state population, in contrast to the $m = 0$ case, where the ground state was mostly occupied. For $m = 2$, a second excited state appears dominantly right above the threshold power, indicating that the two vortex state carries more energy than a single vortex state, as it should. There is a flowless region in the two vortices states, right in between the two vortices, as a result of counterflow canceling each other out. The zero momentum state with excited energy can be seen in this case.

Meanwhile, polariton confinement due to the ring geometry of the non-resonant pumping ($m = 0, +1, +2$) can generate a noticeable feature, in that the excited energy states are discrete [1]. The effective mass of the polariton being $8 \times 10^{-5} m_e$, a few μm confinement should produce the observed energy gap of around 1.3 meV between the two successive states. This is consistent with our ring-shaped beams having roughly $10 \mu\text{m}$ diameter.

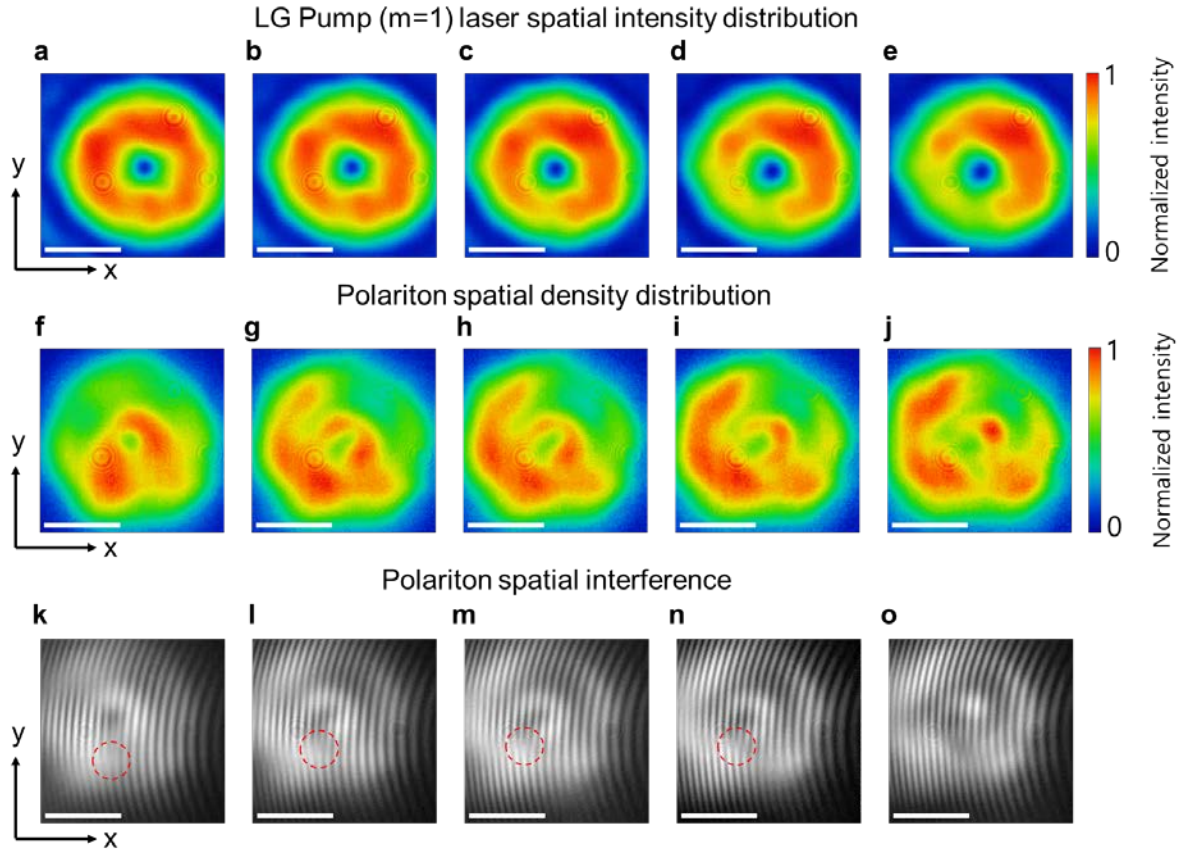


FIG. 3. Stability of the vortex while changing toward the asymmetric spatial distributions of the LG pump (OAM, $m = +1$) spatial intensity and polariton density, considering the spatial interference of the polaritons. (a-e) The LG pump laser intensity distribution was changed toward a more asymmetric shape from a (ring shape) to e (an asymmetrically collapsed ring shape) by manipulating the spatial position of the phase mask on the pump beam path in the experiment setup. The pump laser beam diameter, about $30 \mu\text{m}$. (f-j) The polariton spatial density distribution varied from f (ring shape pumping) to j (asymmetrically collapsed ring shape pumping) toward the asymmetric shape. (k-o) Spatial interference image of the polariton condensate, corresponding to (f-j). A single vortex (red circle, for k-shape interference pattern) was created. (o) No vortex was observed in the spatial interference of the polariton spatial distribution (j). Correspondence relationship: (a→f→k), (b→g→l), (c→h→m), (d→i→n), (e→j→o). These interference images were measured by MZ interferometer. All scale bars, $10 \mu\text{m}$.

III. STABILITY OF VORTEX WHILE CHANGING TOWARD THE ASYMMETRIC SPATIAL INTENSITY DISTRIBUTIONS OF THE LG PUMP BEAM

The stability of the vortex generated by the OAM transfer was further tested using laser beam shapes with a broken circular symmetry. By progressively offsetting the center of the Gaussian beam with respect to the center of the $m = 1$ phasemask, the LG pump beam's spatial intensity distribution became asymmetric, as shown in Fig. 3a-e. The pumping power of the Gaussian beam was fixed to $P = 2P_{\text{th}}$. With a sufficiently large beam spot, the overall OAM of light coming through the phasemask was maintained at $m = 1$, up to a point, and only the spatial intensity distribution was affected.

In return, the spatial density distributions of the polaritons varied, as shown from Fig. 3f-j, in response to Fig. 3a-e. In Fig. 3f, when the Gaussian shape pump beam is focused on the center of the phasemask in the experiment setup, polariton density is fairly isotropic, showing a density depleted region in the center.

Fig. 3g-j shows the distortion in the polariton density, causing the ring-shaped distribution to evolve into a horseshoe shape. Fig. 3k-n shows that one fork-shaped interference pattern of the phase winding (red dashed circles in the figure) appears in the vicinity of the polariton density depleted region. When the pump beam shape is distorted to the point of what is shown in Fig. 3e, the vortex vanishes. (See Fig. 3o.)

A comparison of the laser intensity (Fig. 3a-e) and the polariton emission (Fig. 3f-j) shows that the polariton emission is brighter in the region where the laser is dimmer. This suggests that polaritons are being pushed away from the high laser intensity region. An asymmetrical pump intensity distribution in real space can weaken the stable trap of the polariton vortex and the transfer of the optical OAM in the center of the LG pumping region.

The normalized intensity distribution can be used to visualize the asymmetrical modification of the LG beams between Fig. 3a and 3e. When comparing the intensity difference along the ring shape in Fig. 3a (low-intensity imbalance) and 3e (high-intensity imbalance), it can be seen that as long as the pump intensity imbalance was below 14% along the ring geometry, the vortex survived. The vortex disappeared for an asymmetry greater than 14% (Fig. 3o). From this, we could test how much of the geometrical modification in the spatial intensity distribution of the laser pump with OAM affects the stability of the vortex. These results could be further developed to obtain dynamic control of the vortices by beam shaping of the non-resonant optical pumping.

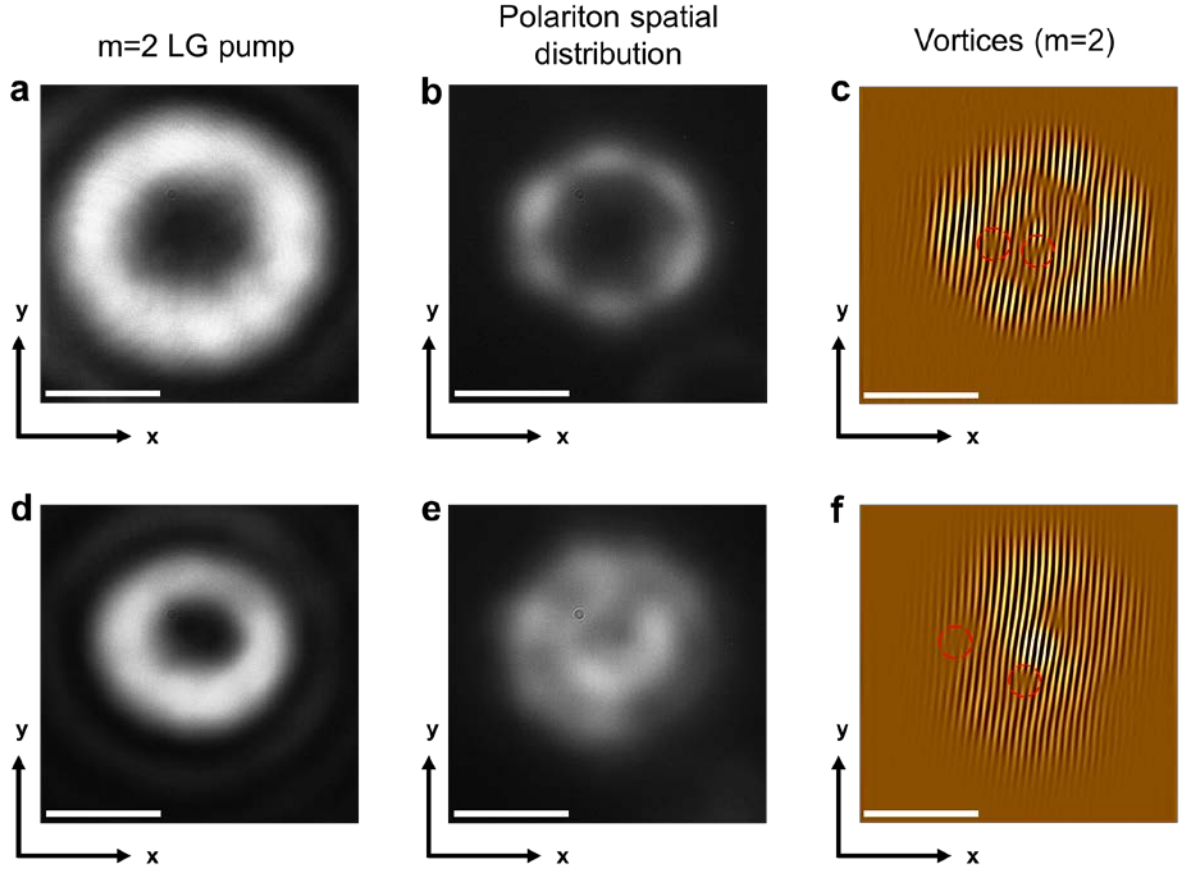


FIG. 4. Stability of transferring the light's orbital angular momentum as a function of the pump beam radii between $7.5 \mu\text{m}$ (large) and $5 \mu\text{m}$ (small) with $m = +2$ LG beam. Scale bar, $10 \mu\text{m}$. (a) The $m = +2$ LG pump laser intensity spatial distribution with a $7.5 \mu\text{m}$ radius. Pump power, 3 mW . (b) Polariton spatial distribution under laser pumping in (a). (c) Polariton spatial interference image in Michelson interferometer under laser pumping in (a). Red circles indicate the location of vortices (c, f). Two vortices were generated inside the LG beam pumping region. (d) $m = 2$ LG pump laser intensity spatial distribution with $5 \mu\text{m}$ radius. Pump power, 3 mW . (e) Polariton spatial distribution under laser pumping in (d). (f) Polariton spatial interference image under laser pumping in (d). One of the two generated vortices was located in the boundary area of the LG beam pumping. The other vortex was located inside the LG beam pumping region. Scale bar $10 \mu\text{m}$.

IV. STABILITY OF TRANSFERRING LIGHT'S ORBITAL ANGULAR MOMENTUM AS A FUNCTION OF THE PUMP BEAM RADIUS.

In order to resolve whether the origin of the vortex formation was the polariton mode selection caused by the spatial pump beam size dependence or the transfer of the optical OAM, the LG pump beam radius was varied from 5 to $7.5 \mu\text{m}$. We performed an experiment by changing the pump beam size with a fixed pump power of 3 mW . With an $m = 2$ phase mask, a condensate with two vortices was formed. Fig. 4a is a spatial distribution image of a laser beam with a beam radius of $7.5 \mu\text{m}$. And Fig. 4b is a fluorescence (polariton

spatial distribution) image and Fig. 4c is the (spatial) interference of the polariton fringe image. Fig. 4d-f are images of the beam radius of 5 μm , respectively. For a pump beam (doughnut shape) size of roughly 170 μm^2 , fluorescence from the polariton condensate has an annular shape with a dark region in the middle. Two vortices reside in this central dark region.

However, when we decreased the pump beam size to 95 μm^2 , the dark region was plugged up by exciton-polaritons. In this case, one of the vortices was pushed out from center to the outside of the region by outward polariton flow, as seen in Fig. 4f. When the beam size was smaller than 95 μm^2 , only one vortex was seen, since the other one was eventually pushed out of the field of view.

If the vortices had been induced by a flow around the sample defects, the vortices would likely be pinned to the defects. The fact that vortices get pushed around in our experiment supports that there is no defect nearby, and the vortices were induced by the angular momentum of the pump beam.

Also, the vortex number was found to match the laser vortex number in the specific beam size region, even when the beam size was changed. Our result is in stark contrast to a recent theoretical prediction [2]. The model predicted that an annular shaped beam with $m = 0$ can produce quantized vortices by mode selection, in which case the number of vortices should show ring size dependence. However, when we used $m = 2$, we could confirm that the vortex number of the exciton-polariton was robustly maintained in beam sizes ranging from 95 to 170 μm^2 . This strongly supports that the vortex formation in our experiment was not due to the geometric effect of the incident beam, but rather the OAM of the laser.

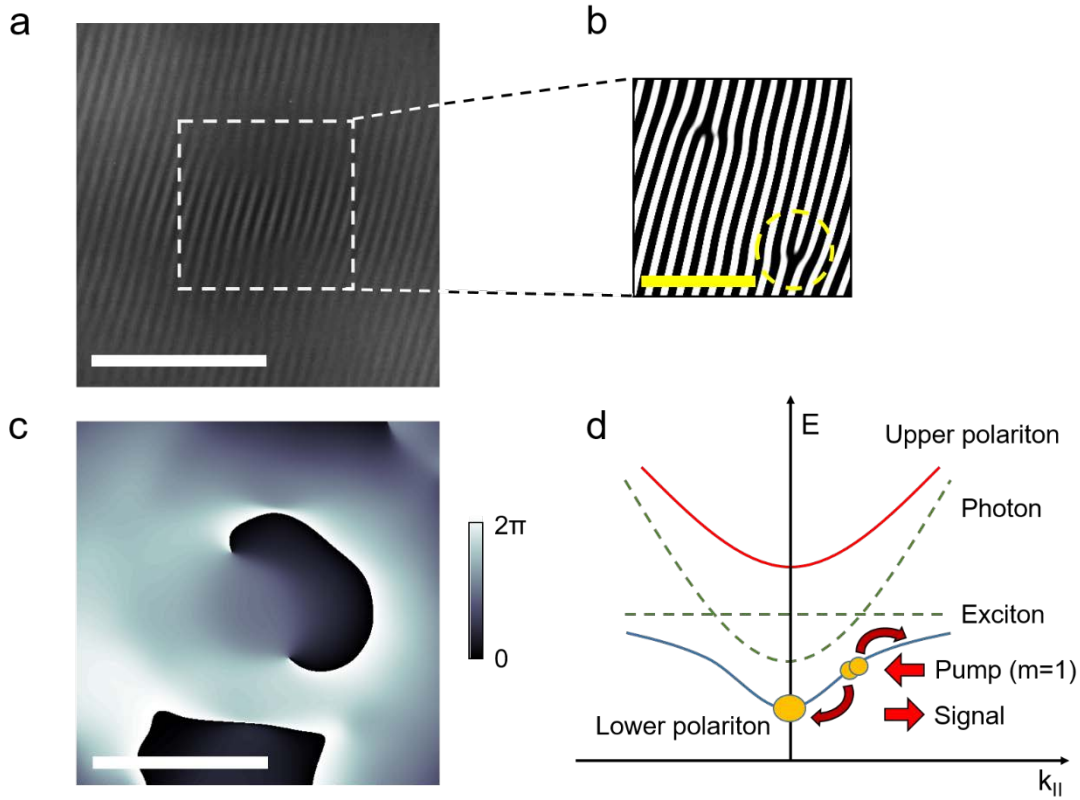


FIG. 5. Creation of a single vortex in an optical parametric oscillator (OPO) pump with 2π phase winding. (a) Spatial interference of the $m = +1$ vortex generated from an OPO pump in the center area of the image in the Michelson interferometer. (b) Magnified image of the dashed square region in a. In the paired fork interference patterns, the one marked by a white circle indicates the real $m = +1$ vortex, and the other is an artifact due to the retro-reflector in the Michelson interferometer. (c) Phase map extracted from a, including 2π phase winding of vortex. (d) OPO pumping conceptual scheme in the energy-momentum dispersion. Scale bar, $10 \mu\text{m}$. Pump beam size is $30 \mu\text{m}$.

V. ANGULAR MOMENTUM TRANSFER IN RESONANT PUMP

To compare different vortex generating methods, we performed an optical parametric oscillator (OPO) scheme with an $m = +1$ phasemask. We injected the pump beam at the inflection point of the lower polariton branch dispersion curve, and the pump beam was a Laguerre-Gaussian beam with the OAM, $m = +1$. In this scenario, the polariton pairs scatter to the signal and idler states of the lower polariton branch through coherent polariton scattering. The pump spot is carefully chosen so that the signal state coincides with the zero momentum ground state of the dispersion curve. Because condensation which is produced by the OPO resonant pump does not experience scattering with the incoherent reservoir, the coherence is known to survive better.

Also, due to the small energy difference between the ground state and the pump state, the resonant OPO pump scheme has little relaxation process from the pump to the final state. The pump beam's OAM is preserved during

the resonant scattering process within the lower polariton branch. When the $m = +1$ state is scattered into the signal state, we can observe the quantized vortex, as shown in Fig. 5a,b.

Our method of generating vortices with non-resonant pumping has distinct advantages over the OPO technique. The nonresonant method does not require pumping the system with a particular momentum and energy known as the magic angle. It is also easier to separate polariton luminescence from laser reflection, as they have noticeably different wavelengths.

REFERENCES

- [1] R. Dall, M. D. Fraser, A. S. Desyatnikov, G. Li, S. Brodbeck, M. Kamp, C. Schneider, S. Höfling and E. A. Ostrovskaya, *Creation of Orbital Angular Momentum States with Chiral Polaritonic Lenses*. *Phys. Rev. Lett.* **113**, 200404 (2014).
- [2] A. V. Yulin, A. S. Desyatnikov and E. A. Ostrovskaya, *Spontaneous formation and synchronization of vortex modes in optically induced traps for exciton-polariton condensates*. *Phys. Rev. B* **94**, 134310(2016)